

Study of freshly excised brain tissues using terahertz imaging

Seung Jae Oh,^{1,8} Sang-Hoon Kim,¹ Young Bin Ji,² Kiyoung Jeong,³
Yeonji Park,¹ Jaemoon Yang,⁴ Dong Woo Park,⁵ Sam Kyu Noh,⁵ Seok-Gu Kang,⁶
Yong-Min Huh,^{1,4} Joo-Hiuk Son,^{7,9} and Jin-Suck Suh^{1,4,*}

¹YUMS-KRIBB Medical Convergence Research Institute, College of Medicine, Yonsei University, Seoul 120-752, South Korea

²Yonsei Institute of Convergence Technology, Yonsei University, Seoul 120-752, South Korea

³Nanomedical National Core Research Center, Yonsei University, Seoul 120-749, South Korea

⁴Department of Radiology, College of Medicine, Yonsei University, Seoul 120-752, South Korea

⁵Nano Materials Evaluation Center, Korea Research Institute of Standards and Science, Daejeon 305-340, South Korea

⁶Department of Neurosurgery, Severance Hospital, Yonsei University College of Medicine, Seoul 120-752, South Korea

⁷Department of Physics, University of Seoul, Seoul 130-743, South Korea

⁸issac@yuhs.ac

⁹joohiuk@uos.ac.kr

*jss@yuhs.ac

Abstract: We demonstrated that tumors in freshly excised whole brain tissue could be differentiated clearly from normal brain tissue using a reflection-type terahertz (THz) imaging system. THz binary images of brain tissues with tumors indicated that the tumor boundaries in the THz images corresponded well to those in visible images. Grey and white-matter regions were distinguishable owing to the different distribution of myelin in the brain tissue. THz images corresponded closely with magnetic resonance imaging (MRI) results. The MRI and hematoxylin and eosin-stained microscopic images were investigated to account for the intensity differences in the THz images for fresh and paraffin-embedded brain tissue. Our results indicated that the THz signals corresponded to the cell density when water was removed. Thus, THz imaging could be used as a tool for label-free and real-time imaging of brain tumors, which would be helpful for physicians to determine tumor margins during brain surgery.

©2014 Optical Society of America

OCIS codes: (170.6795) Terahertz imaging; (170.3880) Medical and biological imaging

References and links

1. J.-H. Son, "Terahertz electromagnetic interactions with biological matter and their applications," *J. Appl. Phys.* **105**(10), 102033 (2009).
2. S. Sy, S. Huang, Y.-X. J. Wang, J. Yu, A. T. Ahuja, Y.-T. Zhang, and E. Pickwell-MacPherson, "Terahertz spectroscopy of liver cirrhosis: investigating the origin of contrast," *Phys. Med. Biol.* **55**(24), 7587–7596 (2010).
3. D. A. Crawley, C. Longbottom, B. E. Cole, C. M. Ciesla, D. Arnone, V. P. Wallace, and M. Pepper, "Terahertz Pulse Imaging: A Pilot Study of Potential Applications in Dentistry," *Caries Res.* **37**(5), 352–359 (2003).
4. K. W. Kim, K.-S. Kim, H. Kim, S. H. Lee, J.-H. Park, J.-H. Han, S.-H. Seok, J. Park, Y. Choi, Y. I. Kim, J. K. Han, and J.-H. Son, "Terahertz dynamic imaging of skin drug absorption," *Opt. Express* **20**(9), 9476–9484 (2012).
5. R. M. Woodward, V. P. Wallace, R. J. Pye, B. E. Cole, D. D. Arnone, E. H. Linfield, and M. Pepper, "Terahertz pulse imaging of ex vivo basal cell carcinoma," *J. Invest. Dermatol.* **120**(1), 72–78 (2003).
6. J.-B. Masson, M.-P. Sauviat, J.-L. Martin, and G. Gallot, "Ionic contrast terahertz near-field imaging of axonal water fluxes," *Proc. Natl. Acad. Sci. U.S.A.* **103**(13), 4808–4812 (2006).
7. A. J. Fitzgerald, V. P. Wallace, M. Jimenez-Linan, L. Bobrow, R. J. Pye, A. D. Purushotham, and D. D. Arnone, "Terahertz pulsed imaging of human breast tumors," *Radiology* **239**(2), 533–540 (2006).
8. J. Y. Park, H. J. Choi, K.-S. Cho, K.-R. Kim, and J.-H. Son, "Terahertz spectroscopic imaging of a rabbit VX2 hepatoma model," *J. Appl. Phys.* **109**(6), 064704 (2011).

9. S. J. Oh, J. Kang, I. Maeng, J.-S. Suh, Y.-M. Huh, S. Haam, and J.-H. Son, "Nanoparticle-enabled terahertz imaging for cancer diagnosis," *Opt. Express* **17**(5), 3469–3475 (2009).
10. S. J. Oh, J. Choi, I. Maeng, J. Y. Park, K. Lee, Y.-M. Huh, J.-S. Suh, S. Haam, and J.-H. Son, "Molecular imaging with terahertz waves," *Opt. Express* **19**(5), 4009–4016 (2011).
11. J. Darmo, V. Tamosiunas, G. Fasching, J. Kröll, K. Unterrainer, M. Beck, M. Giovannini, J. Faist, C. Kremser, and P. Debbage, "Imaging with a Terahertz quantum cascade laser," *Opt. Express* **12**(9), 1879–1884 (2004).
12. S. Kim, F. Hatami, J. S. Harris, A. W. Kurian, J. Ford, D. King, G. Scalari, M. Giovannini, N. Hoyler, J. Faist, and G. Harris, "Biomedical terahertz imaging with a quantum cascade laser," *Appl. Phys. Lett.* **88**(15), 153903 (2006).
13. G. M. Png, R. Flook, B. W.-H. Ng, and D. Abbott, "Terahertz spectroscopy of snap-frozen human brain tissue: an initial study," *Electron. Lett.* **45**(7), 343–345 (2009).
14. Q. T. Ostrom, L. Bauchet, F. G. Davis, I. Deltour, J. L. Fisher, C. E. Langer, M. Pekmezci, J. A. Schwartzbaum, M. C. Turner, K. M. Walsh, M. R. Wrensch, and J. S. Barnholtz-Sloan, "The epidemiology of glioma in adults: a "state of the science" review," *Neuro-oncol.* **16**(7), 896–913 (2014).
15. M. Hefli, H. M. Mehdorn, I. Albert, and L. Dörner, "Fluorescence-guided surgery for malignant glioma: a review on aminolevulinic acid induced protoporphyrin IX photodynamic diagnostic in brain tumors," *Current Medical Imaging Reviews* **6**(4), 254–258 (2010).
16. H. M. Mehdorn, F. Schwartz, S. Dawirs, J. Hedderich, L. Dörner, and A. Nabavi, "High-field ioMRI in glioblastoma surgery - improvement of resection radicality and survival for the patient?" *Acta Neurochir. Suppl. (Wien)* **109**, 103–106 (2011).
17. F. Stockhammer, M. Misch, P. Horn, A. Koch, N. Fonyuy, and M. Plotkin, "Association of F18-fluoro-ethyl-tyrosin uptake and 5-aminolevulinic acid-induced fluorescence in gliomas," *Acta Neurochir. (Wien)* **151**(11), 1377–1383 (2009).
18. R. Weissleder and M. J. Pittet, "Imaging in the era of molecular oncology," *Nature* **452**(7187), 580–589 (2008).
19. R. R. Edelman, J. R. Hesselink, and M. B. Zlatkin, *Clinical Magnetic Resonance Imaging* (Saunders, 1996), Chap. 1.
20. G. I. McIntyre, "Cell hydration as the primary factor in carcinogenesis: A unifying concept," *Med. Hypotheses* **66**(3), 518–526 (2006).

1. Introduction

Terahertz (THz) imaging techniques have been studied as candidates for medical imaging, as they provide a high sensitivity for the detection of interstitial fluid, non-invasiveness, and non-ionizing characteristics [1,2]. Owing to the innate advantages of THz waves, they are suitable for various medical fields, such as dentistry, dermatology, neurology, and oncology [3–12]. THz cancer detection is very promising, and many studies have been performed to diagnose various cancers in the skin, breast, tongue, and liver using THz imaging [5–11]. However, THz imaging is rarely applied for the diagnosis of brain diseases. Investigations of Alzheimer's disease using snap-frozen methods and sliced brain tissue imaging have been reported for post-processed brain tissues but not for whole, fresh brain tissue [11–13].

Glioblastoma is the most common primary brain tumor of the central nervous system [14]. It grows invasively and has unclear margins between the neoplastic and normal regions. Even experienced surgeons cannot increase the rate of complete resection beyond 20% using white-light microscopy [15]. Medical imaging techniques, including neuronavigation, intraoperative magnetic resonance imaging (ioMRI), and positron emission tomography (PET) imaging, have been employed for the past 10 years to determine the exact tumor boundaries during surgery [16,17]. However, the application of such methods in surgery presents several problems. Neuronavigation procedures based on images that are obtained prior to surgery require updated data to account for the intraoperative brain shift during surgery. The ioMRI technique is time-consuming and very expensive. PET imaging not only requires injecting a positron-emitting radionuclide into the body as a tracer but also has a resolution of 2–3 mm, which is low compared with that of MRI or THz, along with a sub-millimeter lateral resolution for clearly determining the tumor margins [5,18]. Recently, fluorescence imaging using protoporphyrin IX induced by 5-aminolevulinic acid has been employed to determine the margin of glioblastoma during the resection of the tumor region [15]. However, fluorescence imaging not only requires suppression of the photodynamic sensitization of the skin and eyes by patient isolation in the dark for over 24 hours but also rarely classifies the tumor region in the early stages, such as grade 2. Additionally, diffraction of visual light

distorts the image. Therefore, label-free imaging methods are necessary to accurately determine the tumor margins in real time.

THz imaging techniques have the potential to determine tumor margins without fluorescent dye in real time. In this paper, we obtained THz images of fresh, whole rat brain tissues with and without glioma and compared the THz imaging results with MRI results. Furthermore, THz images of fresh and paraffin-embedded brain tumors were compared with corresponding hematoxylin and eosin (H&E) stained images to reveal that the differences between the images of normal and cancerous tissues were not caused solely by the water content.

2. Experimental methods

A reflection mode, a THz time-domain system was used to obtain the THz images, as previously shown [8,10]. A mode-locked Ti:sapphire laser with 80-fs pulses at a central wavelength of 800 nm was employed to generate and detect THz pulses. The laser pulses were divided by a beam splitter and focused onto the photoconductive emitter and detector antennae. Ti/Au dipole antennae fabricated on semi-insulated GaAs and low-temperature growth GaAs wafers were used as the emitter and detector, respectively. The generated THz pulses were acquired via the pump-probe sampling method using the convolution function of the THz electrical transient in the detector. The fast optical path delay line with an amplitude of 37 ps and a frequency of 20 Hz was used to obtain THz pulses in real time. The signal-to-noise ratio of time-domain THz waveform reflected at the quartz-metal interface was 1,500, as calculated using the peak-to-peak value of the pulse and the bandwidth of 0.3–1.3 THz. Four parabolic mirrors were used to guide and focus the THz pulses onto the sample, and the incident and reflection angles of the focused beams were both 32 degrees. THz images were obtained while moving the samples on a quartz window. The thickness and diameter of the quartz window were 3 and 50 mm, respectively. A metal thin film was attached on the corner of the scanning window to obtain the reference reflection signal of each THz image.

An orthotopic glioma model for a rat was used as the brain tumor animal model. Unlike a general glioma tumor, this model has a clear boundary between the normal and abnormal regions, such that the determination of the tumor margins is feasible in fresh tissue. Animal models were established by surgically implanting 9L/lacZ rat glioma cells into male 9-week-old Sprague-Dawley rats. The tumors were allowed to grow for 3–4 weeks and monitored by T2-weighted MRI. When the tumors reached 1 cm³ in size, the rat brains were extracted after euthanasia. The extracted whole brains were divided equally in the transverse plane using a knife. All animal experiments were conducted with the approval of the Institutional Animal Care and Use Committee, Yonsei University Health System.

3. Results and discussion

Visual, THz, and MR images for fresh whole brain tissues with and without tumors are shown in Fig. 1. We obtained three images of brain tissue with tumors and a single image of normal brain tissue. The THz images were assembled using the peak-to-peak values of the reflected pulses. To compare the normal and cancerous brain tissue quantitatively, the reflection ratio was used, that is, the measured values of the THz reflection images were divided by the peak-to-peak value of the THz pulse reflected from the layer between the metal plate and quartz window. The margins of the tumor could be distinguished clearly from the normal regions in the THz images, and the intensities of the THz signals in the cancerous brain tissue were greater than those for the normal brain tissue. The location and size of the tumor tissues shown in the THz images were similar to those of the corresponding T2-weighted MR images, where the brightness increased with the water content of the tissue [19]. The brightness of the MR images in the tumor regions was higher than that for the normal regions, indicating that the water content in the cancerous brain tissue was greater than that in the normal tissue. The increase in the water content in the tumor region was caused by complex

biological events such as newly generated blood vessels and body fluid around necrotic debris [20]. The obtained MR and THz images indicates that water can be used as the primary agent in THz brain tumor imaging, as is the case for THz skin cancer imaging [5]. THz image contrast differences were also discovered in the normal brain tissue image, and these corresponded with the grey and white matter areas, as shown in Fig. 1(d). The amplitude of the THz signal was low for the regions where the tissue color in both visual images was white. This is due to the myelin in the white matter. Myelin around the axon of a neuron is mainly composed of a lipid, whose absorbance and reflectivity of THz waves are significantly lower than those of water. As the myelin concentration increased, the visible color became white, and the THz reflection signal decreased. The distribution of white matter in the THz images, which can be used to visualize myelination characteristics, was similar to those in the corresponding T2-weighted MR images. These results indicate that THz imaging is useful not only to detect brain tumors but also to study the qualitative structure of the brain.

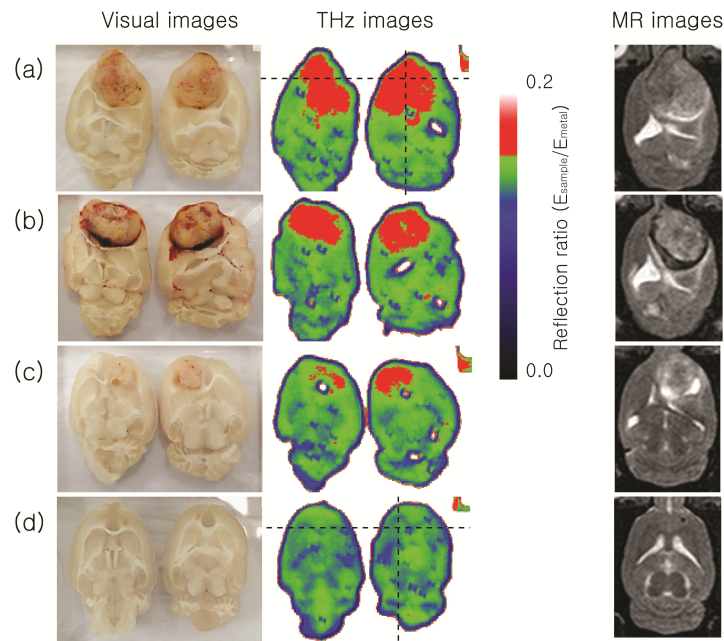


Fig. 1. Visual, THz, and MR images of whole brain images with (a–c) and without (d) tumors. THz image size was $4 \times 3 \text{ cm}^2$; scanning resolution was $250 \mu\text{m}$.

Figure 2 shows the reflection ratio of the peak-to-peak values at the horizontal and vertical lines of Figs. 1(a) and 1(d). For the cancerous brain tissue, the reflection ratio of the tumor region was greater than 14.2%, whereas the reflection ratios for the normal brain tissues were rarely greater than 14.2%. Using the threshold value of 14.2% to differentiate tumors from normal tissue, binary images of the brain tissues were obtained, as shown in Fig. 3. The margins of the tumors in the THz images corresponded to those of real tumors, as shown in Fig. 1, and the tumor signals were rarely found in the normal brain regions. These results indicate that THz imaging potentially offers highly reliable quantitative diagnostic tumor images regardless of the contrast of the white and grey matter. The THz imaging technique could be a useful tool to determine the margins of glioma during the resection of the tumor region and complement conventional fluorescence imaging techniques.

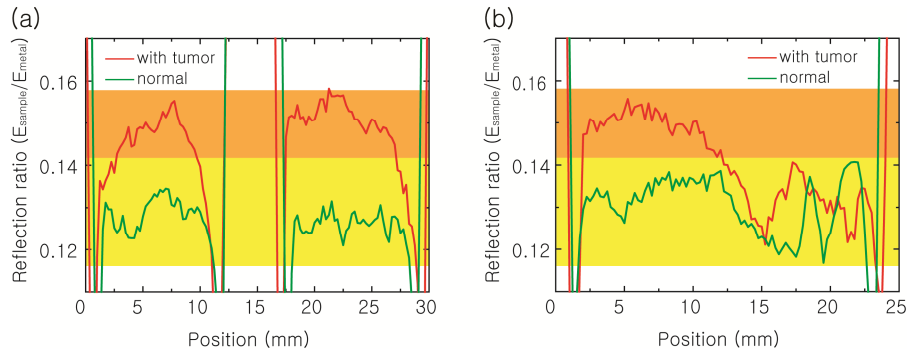


Fig. 2. Reflectivity of the peak-to-peak values of THz pulses on the horizontal and vertical lines of Figs. 1(a) and 1(d). (a) THz values of the horizontal lines of Figs. 1(a), 1(d). (b) THz values of the vertical lines of Figs. 1(a) and 1(d). Yellow region shows that the THz reflectivity ranges from 11.8% to 14.2%. Orange region spans from 14.2% to 15.9%.

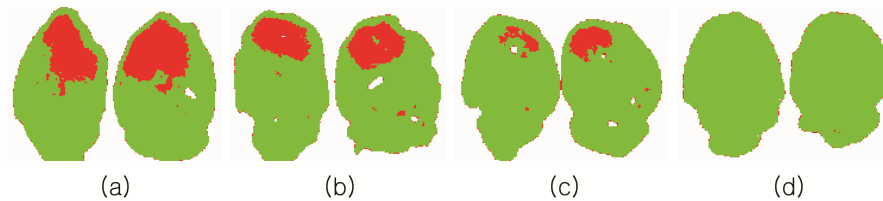


Fig. 3. THz binary images of whole brain with and without tumors. (a), (b), (c): THz binary images of Figs. 1(a), 1(b), and 1(c) respectively. (d) THz binary image of Fig. 1(d). All binary images were separated by the standard percentage of 14.2%.

We investigated which factors could affect the contrast of the THz brain images at the cellular level, aside from water. Few studies have reported that THz medical diagnostic imaging can be achieved using either the physical properties of cells or tissues, such as structure or density, or the chemical properties, such as protein or ion concentrations [1,2,6,8]. Moreover, the THz image contrast for biomedical tissues had not yet been investigated at the cellular level with differences in water content. To perform this experiment, fresh brain tissues were dehydrated by replacing the water with paraffin. The paraffin block was sliced into 3- μm -thick sections, and the sections were stained with H&E to examine the differences between the normal and cancerous tissues at the cellular level. The THz and H&E images of the paraffin-embedded brain tissues with tumors are shown in Fig. 4.

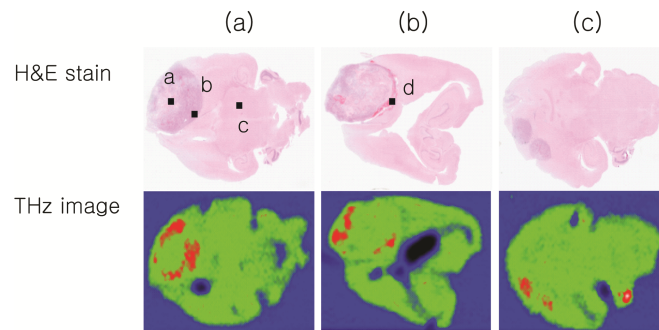


Fig. 4. Comparison between pathology and THz images of paraffin-embedded whole brains with tumors. (a), (b), (c): H&E-stained visual images of the corresponding paraffin-embedded samples of Figs. 1(a), 1(b), and 1(c), respectively. THz images were constructed using the peak-to-peak values of the THz pulses. THz image size was $3 \times 2 \text{ cm}^2$.

Although the reflected THz signals of the tumorous regions were stronger than those of the normal brain tissues, the boundaries of the tumors were only distinguished on the THz

images of the paraffin-embedded brain tissues in Figs. 4(a) and 4(b), whereas the THz image of Fig. 4(c) shows the entire tumor region. The difference in the average signal between the normal and tumor regions for the fresh brain tissues was four times larger than those for the paraffin-embedded brain tissues. The difference between the THz brain images with and without water implies that biological factors besides the water content act as imaging agents.

H&E-stained microscopic images were obtained at the center and boundary of the tumor and normal regions and the area of hemorrhage in the vicinity of the tumor to investigate imaging factors other than water at the cellular level, as shown in Fig. 5. We found that the cell density in the boundary region between the tumor and normal tissue was greater than those at the center of the tumors and in the normal-tissue region. The area of hemorrhage contains many cells, including red blood cells. These results indicate that the THz signals responded to the density of the cells when the effect of water was eliminated. Moreover, histological data indicated that the proliferation of the cells was largely concentrated in the outer region of the tumor, and the center of the tumor was filled with necrotic debris and body fluid water rather than active cells. Thus, although the cell density at the center of the tumor was low, THz signals for fresh tumor tissues were stronger than those for normal tissue.

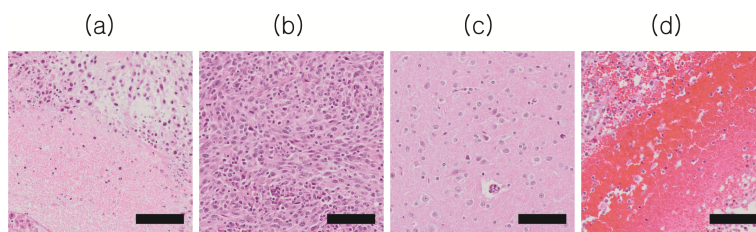


Fig. 5. H&E-stained microscope images of four points on Figs. 4(a) and 4(b). (a) Microscope image of a center of a tumor in Fig. 4(a). (b) Outer region of tumor in Fig. 4(a). (c) Normal region in Fig. 4(a). (d) Hemorrhage region in Fig. 4(b). Black scale bars indicate a length of 50 μm .

4. Conclusion

We obtained THz reflection images of brain tissues with and without tumors via THz imaging and classified all tumor regions. The THz reflection intensity was higher in brain tumors than in normal tissue. The difference in the THz reflection intensity between the normal and tumor brain tissues was adopted to standardize the diagnosis of cancer by exploiting the THz imaging method. Our results indicated that the THz imaging technique could be useful for diagnosing brain tumors. THz imaging could be employed as a complementary technique allowing surgeons to determine tumor margins with a label-free and diagnostic imaging method in real time. The distributions of grey and white matter could readily be identified, suggesting that THz imaging could be used to study brain structure. Furthermore, we showed that the THz contrast between normal and cancerous brain tissues can be distinguished not only by differences in the water content but also by differences in the cell density.

Acknowledgment

This study was supported by a grant from the Korean Health Technology Research and Development Project of the Ministry for Health, Welfare and Family Affairs, Republic of Korea (HI10C19110300) and the National Research Foundation of Korea (NRF) grants funded by the Ministry of Education Science and Technology, Republic of Korea (2012R1A2A1A01011328, and 2012R1A2A2A01047402).